



HAL
open science

Geochemistry of an endorheic thalassohaline ecosystem: the Dziani Dzaha crater lake (Mayotte Archipelago, Indian Ocean)

G rard Sarazin, Didier J z quel, Christophe Leboulanger, Eric Fouilland,
Emilie Le Floc'H, Marc Bouvy, Emmanuelle G rard, H l ne Agogu , C cile
Bernard, Myl ne Hugoni, et al.

► To cite this version:

G rard Sarazin, Didier J z quel, Christophe Leboulanger, Eric Fouilland, Emilie Le Floc'H, et al..
Geochemistry of an endorheic thalassohaline ecosystem: the Dziani Dzaha crater lake (Mayotte
Archipelago, Indian Ocean). *Comptes Rendus G oscience*, 2020, 10.5802/crgeos.43 . hal-03252301

HAL Id: hal-03252301

<https://hal.science/hal-03252301v1>

Submitted on 7 Jun 2021

HAL is a multi-disciplinary open access archive for the deposit and dissemination of scientific research documents, whether they are published or not. The documents may come from teaching and research institutions in France or abroad, or from public or private research centers.

L'archive ouverte pluridisciplinaire **HAL**, est destin e au d p t et   la diffusion de documents scientifiques de niveau recherche, publi s ou non,  manant des  tablissements d'enseignement et de recherche fran ais ou  trangers, des laboratoires publics ou priv s.



INSTITUT DE FRANCE
Académie des sciences

Comptes Rendus

Géoscience

Sciences de la Planète


Gérard Sarazin, Didier Jézéquel, Christophe Leboulanger, Eric Fouilland, Emilie Le Floch, Marc Bouvy, Emmanuelle Gérard, Hélène Agogué, Cécile Bernard, Mylène Hugoni, Vincent Grossi, Marc Troussellier and Magali Ader

Geochemistry of an endorheic thalassohaline ecosystem: the Dziani Dzaha crater lake (Mayotte Archipelago, Indian Ocean)

Volume 352, issue 8 (2020), p. 559-577.

<https://doi.org/10.5802/crgeos.43>

© Académie des sciences, Paris and the authors, 2020.
Some rights reserved.

 This article is licensed under the
CREATIVE COMMONS ATTRIBUTION 4.0 INTERNATIONAL LICENSE.
<http://creativecommons.org/licenses/by/4.0/>



*Les Comptes Rendus. Géoscience — Sciences de la Planète sont membres du
Centre Mersenne pour l'édition scientifique ouverte
www.centre-mersenne.org*



Original Article — Petrology, Geochemistry

Geochemistry of an endorheic thalassohaline ecosystem: the Dziani Dzaha crater lake (Mayotte Archipelago, Indian Ocean)

Gérard Sarazin^{* a}, Didier Jézéquel^a, Christophe Leboulanger^b, Eric Fouilland^b, Emilie Le Floch^b, Marc Bouvy^b, Emmanuelle Gérard^a, Hélène Agogué^c, Cécile Bernard^d, Mylène Hugoni^e, Vincent Grossi^f, Marc Troussellier^b and Magali Ader^a

^a Université de Paris, Institut de Physique du Globe de Paris, CNRS, F-75005 Paris, France

^b UMR 9190, MARBEC, CNRS-Université de Montpellier -IRD - IFREMER, 34095 Montpellier Cedex 5, France

^c UMR 7266 LIENSs, La Rochelle Université–CNRS, 17000 La Rochelle, France

^d Muséum National d'Histoire Naturelle, CP 39, 75231 Paris cedex 05, France

^e Univ Lyon, Université Claude Bernard Lyon 1, CNRS, INRAE, VetAgro Sup, UMR Ecologie Microbienne, F-69622 Villeurbanne, France

^f Univ Lyon, Univ Lyon 1, CNRS, ENSL, Laboratoire de Géologie de Lyon : Terre, Planètes, Environnement, F-69622 Villeurbanne, France

E-mails: gsarazin@gmail.com (G. Sarazin), jezequel@ippg.fr (D. Jézéquel), christophe.leboulanger@ird.fr (C. Leboulanger), eric.fouilland@cnrs.fr (E. Fouilland), emilie.lefloch@univ-montp2.fr (E. Le Floch), marc.bouvy@ird.fr (M. Bouvy), emgerard@ippg.fr (E. Gérard), helene.agogue@univ-lr.fr (H. Agogué), cecile.bernard@mnhn.fr (C. Bernard), mylene.hugoni@univ-lyon1.fr (M. Hugoni), Vincent.Grossi@univ-lyon1.fr (V. Grossi), troussel@univ-montpl2.fr (M. Troussellier), ader@ippg.fr (M. Ader)

Abstract. Dziani Dzaha is a maar the age of which is close to 4000 years. While its water is thought to have originated from seawater it is now considered as an extreme environment due to its hypersaline and alkaline characteristics. Those extreme features have led to the simplification of the trophic network. Cyanobacteria account for up to 95% of the photosynthetic biomass. The main biogeochemical processes, *i.e.* photosynthesis, bacterial sulfate reduction and methanogenesis could explain the current water composition. As far as we know, this ecosystem could be unique on Earth, extending the nature and chemical limits of aquatic inland ecosystems.

Keywords. Thalassohaline lake, Endorheic ecosystem, Cyanobacteria, Methane emission, Biogeochemistry, Mayotte.

Manuscript received 31st July 2020, revised and accepted 24th November 2020.

* Corresponding author.

1. Introduction

The Dziani Dzaha is a small tropical lake of volcanic origin (maar) hosted in a crater formed by a phreatomagmatic eruption that likely occurred between 7000–4000 years BP [Zinke *et al.*, 2003] on Petite Terre, an island of Mayotte archipelago (Northern Mozambique Channel, Western Indian Ocean). The lake surface extends at ≈ 0 m above sea level. Since this latter remained almost constant in the last 7000 years BP, some authors suggest that seawater was by far the main contributor to the initial filling of lake Dziani Dzaha [Smith *et al.*, 2011]. Subsequent isolation from the ocean made it an endorheic hydrosystem, which evolved with time into a warm, hypersaline and alkaline environment. However, because of its seawater origin, the chemical composition of this lake differs from classic continental alkaline lakes and has been categorized as thalassohaline [Leboulanger *et al.*, 2017].

The Dziani Dzaha ecosystem hosts an atypical biological assemblage, almost exclusively composed of microorganisms, with biomass dominated by two phytoplanktonic species (the picoeukaryote, *Picocystis salinarum*, and the large filamentous cyanobacterium, *Arthrospira fusiformis*; [Bernard *et al.*, 2019, Cellamare *et al.*, 2018]. A diverse heterotrophic prokaryotic community of Archaea and Bacteria complement the microbial community, accompanied with scarce eukaryotic protists [Aucher *et al.*, 2020, Hugoni *et al.*, 2018]; no aquatic metazoans have been detected to date [Hugoni *et al.*, 2018]. By contrast with other tropical saline-alkaline ecosystems where *Arthrospira* profusely develops seasonally (for example in Rift Valley lakes, Krienitz and Schagerl, 2016), no grazing control of planktonic biomass by macroorganisms or drastic seasonal successions in plankton community's composition was identified. Actively growing stromatolites are found on the shores, with Cyanobacteria (mostly *Pleurocapsales* and *Leptolyngbia*) and non-sulfur purple bacteria (mostly *Rhodobacteraceae*) identified in the biofilms [G rard *et al.*, 2018]. These modern microbially-mediated sedimentary structures are living counterparts of the oldest fossil records of life (Late-Archean, Proterozoic oceans). They are scarce in modern marine environments and are mainly encountered in locations where metazoans are excluded as a consequence

of extreme environmental conditions [Rishworth *et al.*, 2017].

The water column of lake Dziani Dzaha shows a vertical physico-chemical structure that affects both the structure and the activities of the different microorganism populations [Bernard *et al.*, 2019, Hugoni *et al.*, 2018, Leboulanger *et al.*, 2017], which in turn may directly or indirectly drive the non-conservative chemical composition of the water column. Among the most remarkable biogeochemical characteristics of the vertical stratification of this lake, is the presence of a thin oxic water surface layer (most of the time less than 1 m thick), originating from the very productive phytoplanktonic community and overlying a permanently anoxic water column [Leboulanger *et al.*, 2017]. This oxic/anoxic stratification, together with the microorganism composition of the ecosystem and the presence of stromatolites, is another feature that the “modern” lake Dziani Dzaha shares with some Precambrian environments after the emergence of oxygenic photosynthesis [Hamilton *et al.*, 2016].

Thus, from a biogeochemical point of view, lake Dziani Dzaha constitutes a fascinating, and maybe unique system, which raises several questions:

- How did the chemical composition of this lake evolve since its initial filling by seawater (<7000 BP)?
- Which elements are conservative or non-conservative? And what are the abiotic and biotic processes involved in the dynamics of the latter?
- Which scenario can be foreseen for the biogeochemical evolution of Dziani Dzaha water?

We here address these questions using the hydrological and geochemical analyses performed during several field surveys from 2012 to 2017. To our knowledge, the present work is the first so far reporting the detailed chemical composition and biogeochemical functioning of lake Dziani Dzaha.

2. Site description: the lake and its watershed

The lake is located on the Petite Terre Island of the Mayotte archipelago. Its geographical coordinates are: 12° 46.237' S and 45° 17.315' E. The lake is elliptical in shape with a major E–W axis of 640 m and

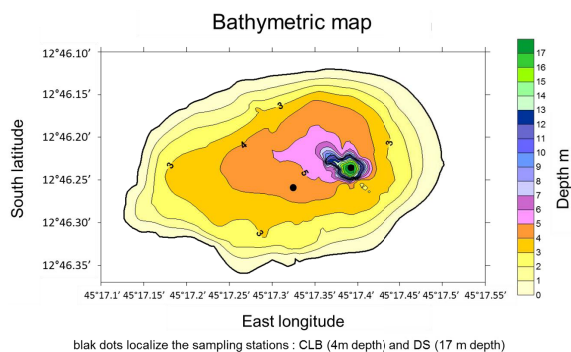


Figure 1. Bathymetric map of the lake. Black dots localize the sampling stations: CLB ca. 4 m depth and DS (deep site) ca. 17 m depth.

a shorter N–S axis of 470 m, and a surface area of 0.236 km². A bathymetric survey was performed in April 2012 using an echo sounder coupled to a GPS (Figure 1).

On the lake central area (CLB sampling station), the water depth varies seasonally, from 3.5 m at the end of the dry season (April to November) to approximately 4 to 4.5 m at the end of the rainy season (December to March). Within a very narrow zone (<100 m² *i.e.* about 0.04% of the lake surface) close to the eastern shore, the water depth reaches 18 m during the rainy season (DS sampling station). It is surrounded by the walls of the crater: ca. 70 m above sea level along the E–W axis and ca. 50 m along the N–S axis. The surface area enclosed in the crater top line accounts for the whole geographic watershed catchment area. It is of approximately 0.5 km². Since the crater slopes are very steep, the watershed surface does not have a great extension compared to that of the lake. However, the cross section published by Sanjuan et al. [2008] shows that the hydrological catchment area has probably a larger surface although it is not possible to evaluate its extension. The petrography of the lake catchment consists of levels of pumice and volcanic ashes in which many decimetric to centimetric fragments of clinkstone are found (Figure in Supplementary 1). Ashes and pumices are of phonolitic composition [Pelleter et al., 2014] with anorthoclase Na_{0.7}K_{0.3}AlSi₃O₈ as the dominant feldspar [Milesi et al., 2019]. It is likely that the volcanic eruption also sputtered the underlying carbonate reef, since ashes and pumices contain numerous fragments of reef reaching up to one meter in size [Milesi et al., 2019].

The high porosity of pumices and ashes favors the infiltration of rain and the supply of dissolved elements into the lake, as well as the probable contribution of particulate detrital matter. This contribution of solid inputs is probably also ensured by the dry fallout for which we have no data.

Several unusual features reinforce the uniqueness of this lake. The most visible one is its deep green color all year round which is due to the extremely high biomass (POC 30–70 mg·L⁻¹) of microbial phytoplankton, especially *Arthrospira fusiformis* that represents up to 95% of the biomass [Bernard et al., 2019, Cellamare et al., 2018, Leboulanger et al., 2017].

The second most visible is the presence, mainly along the South and West shores, of stromatolites, some of them being columnar and emerging from the lake surface during the dry season and usually submerged during the rainy season [G rard et al., 2018].

The third one is the presence in several points of magmatic CO₂ outgassing revealed by bubbles that come bursting onto the surface, some of them being channelized by the columnar stromatolites [Milesi et al., 2019]. Other magmatic CO₂ degassing points have also been reported on two beaches of Petite Terre [Sanjuan et al., 2008, Traineau et al., 2006].

The structure of the water column is controlled by the meteorological parameters, mainly the rainfall: at the end of the rainy season (April to May), owing to the accumulation of soft water, a strong salinity gradient (halocline) develops at around 2 m. During the dry season (June to November) the halocline vanishes and salinity is close to 65 psu whatever the depth. An extensive description of the water column structure is given in Section 5.3.

3. Materials and methods

Although a few samples were collected in 2009, 2010 and 2011 [Leboulanger et al., 2017], most of the fieldwork was performed once to twice a year from April 2012 to November 2017 (except in 2013, no field work). Complete description of sampling and analytical procedures are in Supplementary 2.

4. Results

Data are presented as vertical concentration profiles obtained at the DS station (17 to 18 m depth

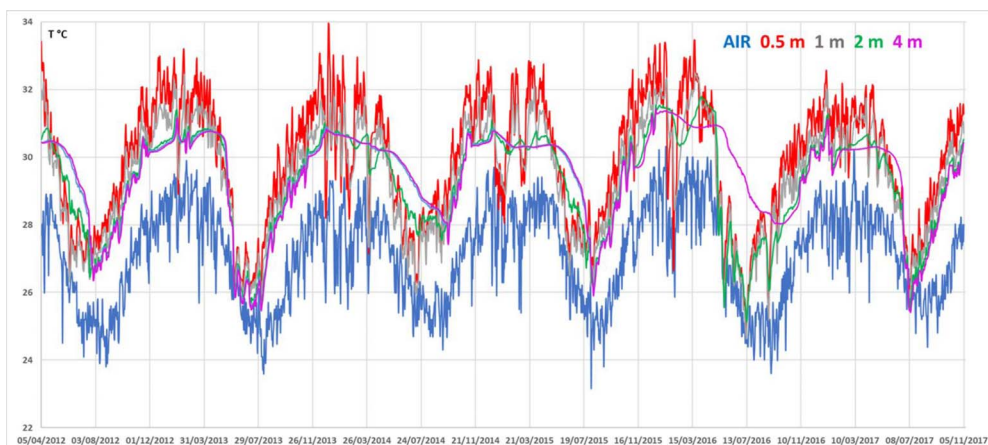


Figure 2. Evolution of air and water column temperatures from April 2012 to November 2017.

depending on the season). Lateral variations of the measured parameters were considered negligible, since the water samples collected at the CLB station (3 to 4 m depth) did not show any significant difference with those collected at the DS station, the same day at the same depth. Results are reported for all the field surveys from April 2012 to November 2017 in Figures 5 to 10.

4.1. *In situ measurements*

Water temperature varied in a clear seasonal pattern (Figure 2): mean summer temperatures (January to March) were around 32 °C at 0.5 m depth, dropping down to 27–28 °C in winter (end of August).

In four occurrences (out of six sequences), the onset of winter resulted in a thermal inversion, with the temperature at 3 and 4 m depth exceeding the temperature of the upper waters. Over the ca. 67 months of recording, the surface temperature of the lake was always above or at least equal to air temperature. Profiles of temperature, pH, salinity, dissolved oxygen (DO) and Eh are shown in Figures 3 and 4. Seasonal alternation resulted in a marked dilution of the salinity in the upper water layer of the lake during the rainy summer periods (from up to 63 psu in November 2017, down to 20 psu in April 2012 since the water sampling was done just after a two days heavy rain fall of 91 mm). The dilution by rainwater induced a sharp halocline between 1.6 and 2 m depth,

as measured in April and August campaigns. This halocline totally vanished after water column mixing, as observed during October–November campaigns (Table 3). This dilution also resulted in a marked increase in pH within the first 2 m below the surface, from almost 9.0 during the dry/non-stratified season to above 9.4 during the rainy/stratified season.

DO concentration and redox potential (Eh) profiles are not unequivocally affected by the seasonal variation, but exhibit a consistent pattern of decrease from surface to ca. 2–3 m depth in all vertical profiles (Figure 4). Except for November 2014 and 2015, surface DO reached concentrations that largely exceeded dioxygen solubility during the day, as a result of intense photosynthetic activity of cyanobacteria in the photic layer. Despite high DO concentrations, Eh values are nevertheless notably low (always negative except in the 0.5 m upper layer in April 2015), suggesting a highly reducing environment throughout the whole water column.

4.2. *Major elements*

Figures 5 to 8 display concentration profiles of the main major dissolved species in the water column.

Figure 5 displays the concentration profiles of major cations (Na, K, Ca, Mg). At the end of the rainy season they show a sharp concentration gradient located at the halocline ca. 1.7 to 2.0 m below the surface. Except for calcium for which concentrations are

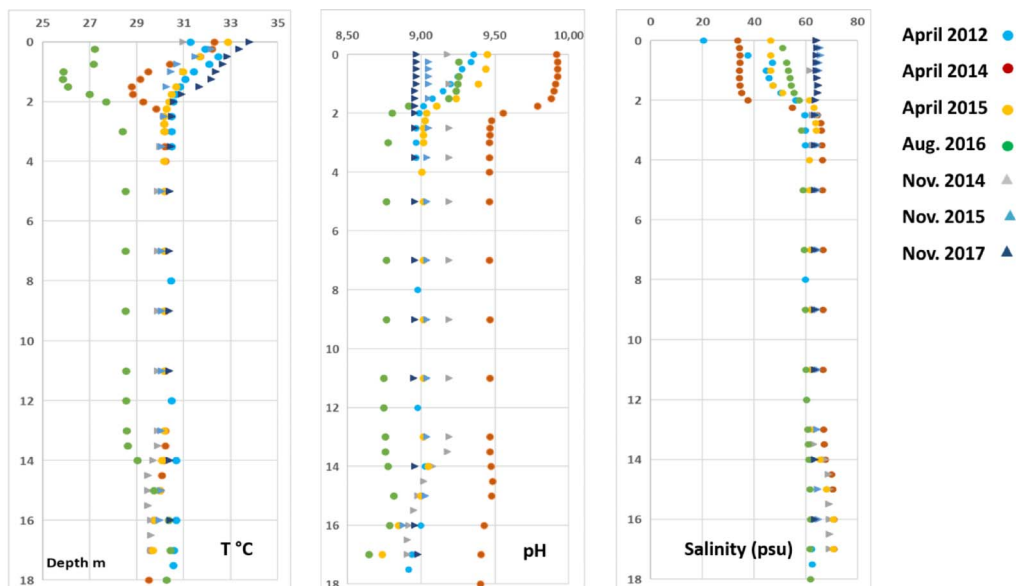


Figure 3. Profiles of in situ measurements: temperature, pH and salinity. Dots and triangles correspond to periods when the water column was stratified (rainy season) or non-stratified (dry season without halocline), respectively.

higher in the surface layer than below the halocline, the others have the same pattern with lower concentrations in the surface layer. For all profiles, except Ca, a slightly marked chemocline is observed at the depth of 13 m.

Profiles of Cl, total dissolved sulfide ($\Sigma S(-II)$ *i.e.* $[H_2S] + [HS^-]$) and alkalinity (Alk) are displayed in Figure 6.

The three profiles show a marked gradient at the depth of the halocline already observed for the major cations. The sharpest gradient concerns the $\Sigma S(-II)$ profile since the concentrations drop to less than a few hundred $\mu\text{mol}\cdot\text{L}^{-1}$ in the upper layer of the water column when it can reach more than $6\text{ mmol}\cdot\text{L}^{-1}$ 0.25 m below the halocline. When halocline is lacking the $\Sigma S(-II)$ concentrations are very low, similar to these observed in the 0–2 m depth at the end of the rainy season.

The depth profiles of sulfate and $\Sigma S(-II)$, from April 2015 are depicted in Figure 7. Whatever the season, the sulfate concentration above the halocline was $2.4 \pm 0.4\text{ mmol}\cdot\text{L}^{-1}$. Below it, the sulfate concentration is lower than the limit of quantification when it is analyzed in water samples where $\Sigma S(-II)$ has been previously eliminated (Figure 7). Therefore, $\Sigma S(-II)$

and SO_4^{2-} profiles reveal a “mirror” behavior of these two species.

The mean DOC concentration in the surface waters is $5300\text{ }\mu\text{mol}\cdot\text{L}^{-1}$ when the halocline exists. When the water column is not stratified the mean concentration is $6800\text{ }\mu\text{mol}\cdot\text{L}^{-1}$ within the same depth range (Figure 7).

4.3. Sediments and stromatolites

The EDAX spectrum of a stromatolite is shown on Figure 8(a). Only calcium carbonates were detected. XRDP analysis revealed the occurrence of both calcite and aragonite.

The very superficial sediment (0–1 cm) collected close to CLB station in 2010 and analyzed by XRDP, consisted in a mixture of aragonite and hydromagnesite (Figure 8(b)) while the sediment collected at the same place, 10 cm below the sediment-water interface (SWI), showed an EDAX spectrum that revealed the presence of inherited silicate minerals (Figure 8(c)). The detection of NaCl (Figures 8(b) and (c)) is an artifact due to incomplete rinsing of pore waters, leading to the crystallization of halite during freeze-drying.

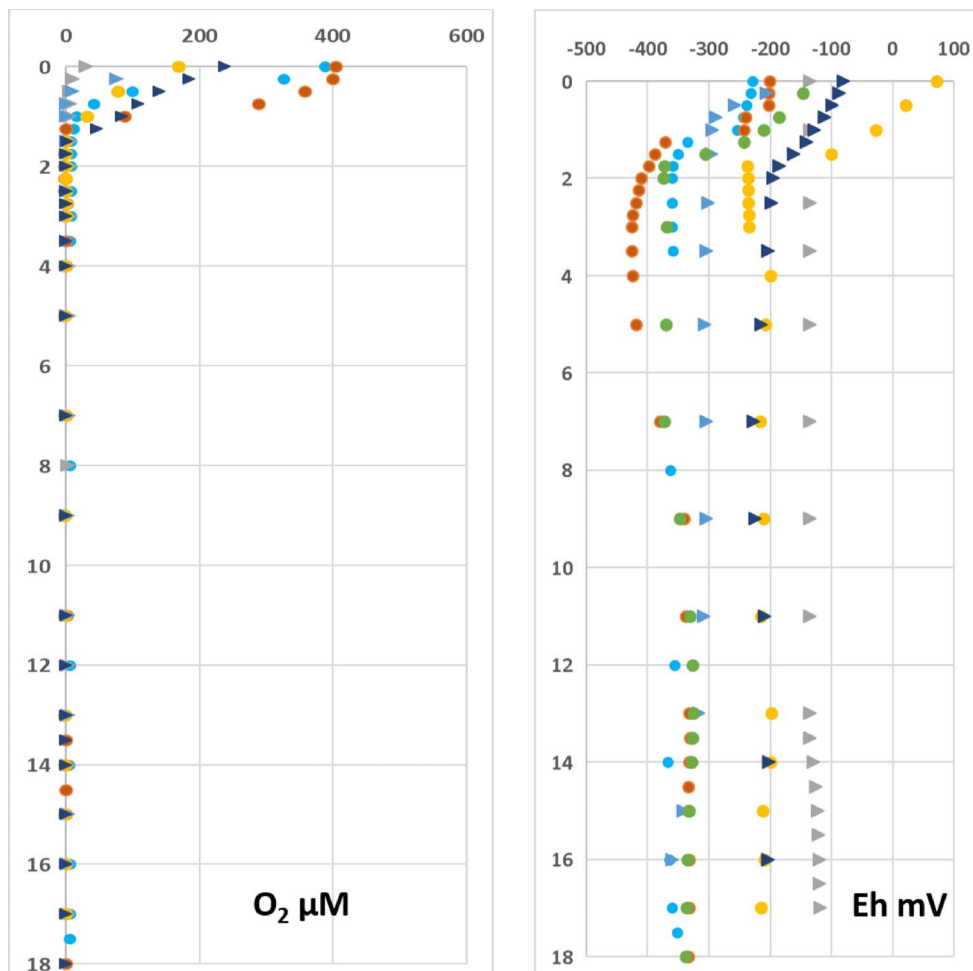


Figure 4. Profiles of in situ measurements: dissolved oxygen (DO) and redox potentiel. Same symbol as Figure 3.

4.4. Gases

4.4.1. Fluxes of CO_2 and CH_4 at the water–air interface

Fluxes of CO_2 and CH_4 measured on the field by the FC method are displayed in Table 1.

These results show that the CO_2 and CH_4 fluxes vary seasonally and are clearly anticorrelated ($r^2 = 0.94$).

4.4.2. CH_4 profiles in the water column

Concentration profiles of CH_4 measured at the DS station in April 2015 and August 2016 (stratified seasons), and November 2015 (non-stratified season) are displayed in Figure 9.

In November 2015, in the absence of halocline, the concentrations were very low (within the range of $100 \mu\text{mol}\cdot\text{L}^{-1}$) along the whole water column, while in April 2015 and August 2016, when the water column is stratified, there was a very strong concentration gradient superimposed on the halocline.

5. Discussion

5.1. Meteorological context and water balance

The temporal evolution of water and air temperatures between April 2012 and November 2017 highlight the marked contrast between a hot and rainy season from ca. December to March and a

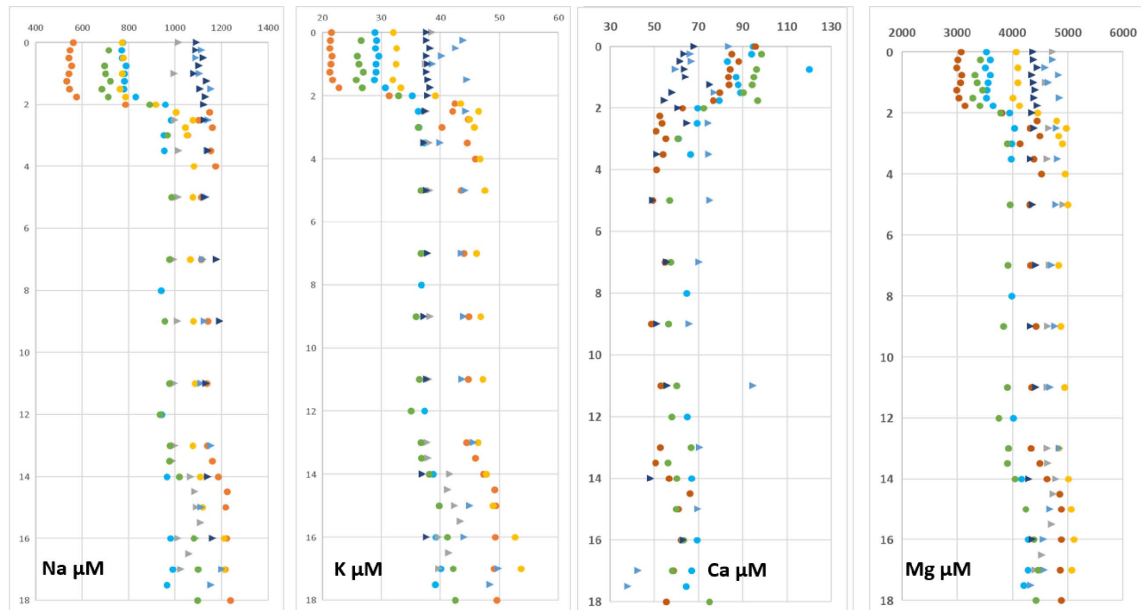


Figure 5. Depth concentration profiles of sodium, potassium, calcium and magnesium. Dots correspond to periods when the water column was stratified (rainy season) while triangles correspond to the period without halocline (dry season).

warm and dry season from ca. April to November (Figure 2).

It is remarkable that the temperature of the air is most of the time lower than that of the water column, which is quite unusual. This particularity is attributable to the permanent dark green color of the water, which promotes heat absorption by reducing the albedo. It is also noticeable that the transition from hot to warm season is accompanied by a more rapid cooling of surface waters, which creates an inverse thermal stratification except in 2013 (Figure 2). However, the thermal gradient is always weak (~ 0.8 $^{\circ}\text{C}/\text{m}$) and do not seem to impact the hydrostatic equilibrium of the water column which is ensured by the salinity gradient (Figure 3).

Irradiance exhibits a low amplitude seasonal variation with a maximum during the hot and rainy season (Supplementary 3). The irradiance average between 05 April 2012 and 31 December 2017 was 231 ± 55 $\text{W}\cdot\text{m}^{-2}$. This shows that the amount of energy, which mainly controls lake water evaporation, is nearly constant through time.

Although we cannot totally exclude the occurrence of direct runoff during exceptional rainstorms such as those of January 2008 (500 mm rainfall within

Table 1. Water-atmosphere fluxes of CO_2 and CH_4 in $\text{mmol}\cdot\text{m}^{-2}\cdot\text{d}^{-1}$

Date	CO_2	CH_4
April 2012	120	92
April 2014	42	136
April 2015	97	103
August 2016	60	107
October–November 2014	220	39
November 2015	211	38

4 days), we consider them as negligible over the course of our six years survey and we assume in the following discussion that the equilibrium of the water system is a balance between direct rainfall, rainfall infiltration lake water infiltration and evaporation.

Data from Julvez [1987] give the average rainfall over a period of 12 years (1984–1996), which is estimated to 1340 $\text{mm}\cdot\text{yr}^{-1}$. Another estimation given by Korzun [1978] for Indian Ocean between 10° and 20° S is 1410 $\text{mm}\cdot\text{yr}^{-1}$. Data from the Pamandzi airport meteorological station (M t o France), collected between January 2012 and December 2017 yield an

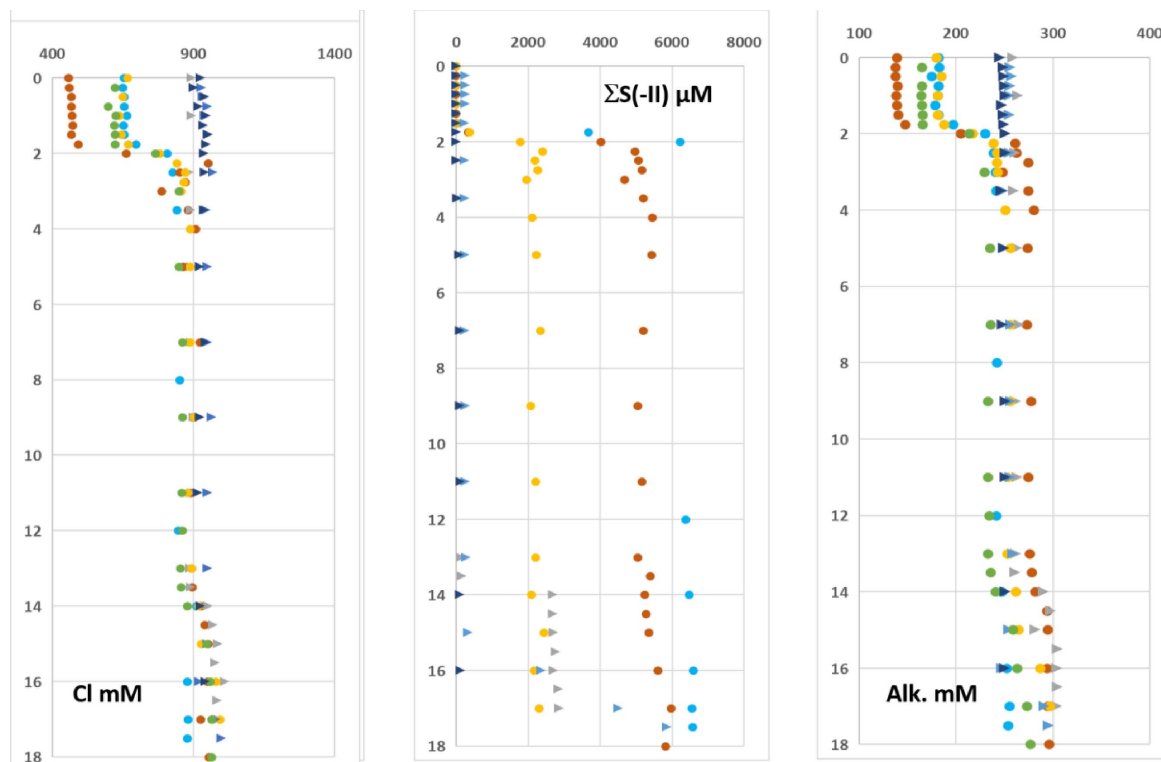


Figure 6. Depth concentration profiles of chloride, dissolved sulfide and alkalinity. Dots and triangles correspond to periods when the water column was stratified (rainy season) or non-stratified (dry season without halocline), respectively.

average of $1247 \text{ mm}\cdot\text{yr}^{-1}$, 8% lower than the Julvez's estimation. However, the rainfall (Supplementary 3) remains subjected to large variations from one year to another as shown in Table 2.

Evaporation is much more difficult to evaluate, except for pure water for which empirical relations can be used (www.thermexcel.com; 2012). For seawater evaporation, published data are scarce. An estimation of $2060 \text{ mm}\cdot\text{yr}^{-1}$ for the Indian Ocean between 10° and 20° S is given by Korzun [1978]. Applied to Dziani Dzaha, this estimation would lead to the lake drying out within a few decades, which is obviously excluded.

Another estimation of water evaporation can be calculated using the relation given by Yu *et al.* [2008] which takes into account the flux of latent heat (Q_{LH}), the water density (ρ_w) and the latent heat of evaporation (L_e) (Supplementary 4). Owing to the uncertainties on Q_{LH} the evaporation is estimated to be 1370 to $1500 \text{ mm}\cdot\text{yr}^{-1}$ which is very close to the estimations

of average rainfall. These features make this lake an endorheic and almost stationary hydrosystem. Nevertheless, the evaporation rate could exceed precipitation and lead to the present-day salinity of the lake, which is concentrated nearly twice with respect to seawater (see discussion in Section 5.3).

Data series obtained from the limnigraph (Supplementary 5) installed on site do not disagree with the hypothesis of a quasi-stationary steady state. It recorded alternate periods of water level fluctuations due to the ratio between evaporation and precipitation and show also that there is a lag time between the rain input and the infiltration that slowly feeds the lake through phreatic waters. The observed linear variations of the lake level with time allow to infer that there is no correlation with the oceanic tide period which, every six hours, induces a mean tidal range close to 3 m in the nearby Mozambique Channel, reinforcing the hypothesis that lake Dziani Dzaha is isolated from the ocean.

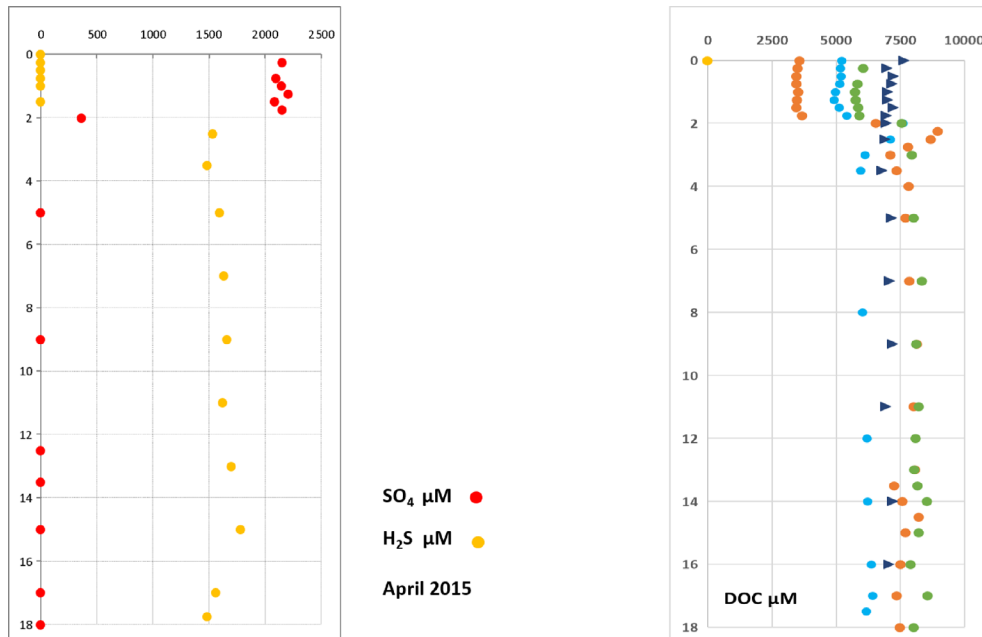


Figure 7. Typical SO_4^{2-} and $\Sigma\text{S}(-\text{II})$ profiles obtained in April 2015. DOC profiles. Dots and triangles correspond to periods when the water column was stratified (rainy season) or non-stratified (dry season without halocline), respectively.

Table 2. Average rainfall recorded between January 2012 and December 2017 at Pamandzi airport station (Petite Terre)

Year	2012	2013	2014	2015	2016	2017
Rainfall (mm)	1310	951	1201	1326	1439	1255

5.2. Water column stratification

According to the season, the water column was either stratified with an upper layer having a lower salinity than the deep layer, or non-stratified when the salinity was homogeneous with depth. The upper layer exhibited a maximum thickness at the end of the rainy season, but the stratification remained until the beginning of the dry season as observed in August 2016 when the lake level was still very high as a consequence of heavy rainfalls (Table 2).

The upper water layer at the end of each rainy season resulted from mixing between low-density rainwater and the much denser deep water, inducing a salinity gradient between 1.75 and 2 m depth (Figure 5).

The CTD, DO, pH and redox profiles (Figures 3 and 4) clearly show that the structure of the water column was dependent on the season. At the end of the rainy season the water column was stratified for all these parameters, which leads to very marked gradients except for the temperature. These gradients were superimposed on the halocline, which precise position depended on the amount of rainfall during the months preceding fieldwork (Table 3). The DO and Eh gradients were located at a smaller depth than the others suggesting that redox processes occurring in the upper layer of the lake generate a strong reducing medium in account of the highly negative Eh values.

At the end of the dry season there were practically no gradients except for DO, Eh and temperature in the vicinity of the surface. It is noteworthy that

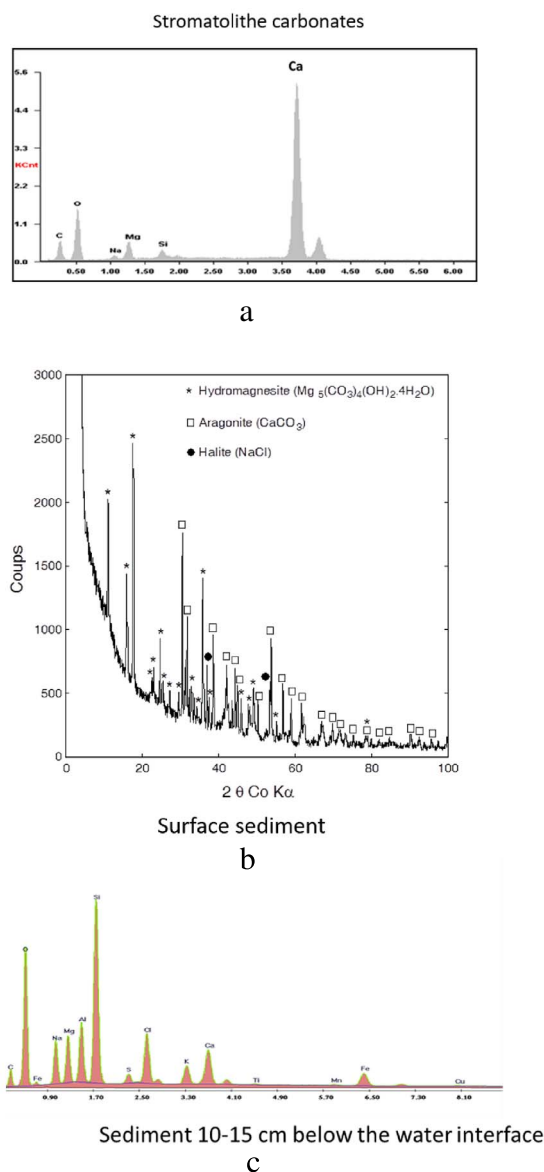


Figure 8. (a) EDAX spectrum of a stromatolite; (b) XRD diagram of superficial sediment where only aragonite and hydromagnesite were detected; (c) EDAX spectrum of subsurface sediment (ca. 10 cm depth) showing the contribution of inherited silicate minerals.

the water column was permanently anoxic at depth (Figure 4), whatever the season. The oxygenated surface layer extended up to 1.25–1.50 m depth in April 2012 and November 2017, when O₂ maximum

Table 3. Cumulated rainfall recorded 2 months before the field campaign

Period	Rain (mm)	Halocline depth (m)
April 2012	670	1.6
April 2014	653	2.0
October 2014	12	None
April 2015	329	2.0
November 2015	10	None
August 2016	16	1.75
November 2017	51	None

In 2016, the rainiest year, rainfalls happened from January to April but the halocline was still present in August.

concentrations were observed, while this layer was much smaller (a few tens of centimeters) and O₂ concentration lower during the non-stratified period excepted in November 2017 (Figure 4). These results can be explained owing to the presence or the lack of halocline. When halocline is present, the sharp salinity/density gradient leads to a drastic reduction of the dispersion coefficients for all dissolved species, therefore O₂ exchanges happen mainly between the lake surface (oversaturated) and the atmosphere. Then, diffusion towards the lake bottom is very low and O₂ is promptly consumed by reducing chemical species, which presence was attested by the very negative values of the Eh. The bulk result being the anoxia of the water column below the halocline. When halocline vanished, there was no remaining diffusion barrier and O₂ could be reduced within the first top centimeters of the water column.

5.3. Origin of the lake water and its evolution towards the present day composition

The hierarchical clustering diagram which compares 50 saline lake waters published by Leboulanger *et al.* [2017] shows that the Dziani Dzaha composition can be convincingly ascribed as having evolved from seawater (thalassosaline lake). We thus assume that the lake quickly filled with seawater after the phreatomagmatic eruption, between 7000 and 4000 yr BP [Zinke *et al.*, 2003], and that its present-day composition results from yearly cycles

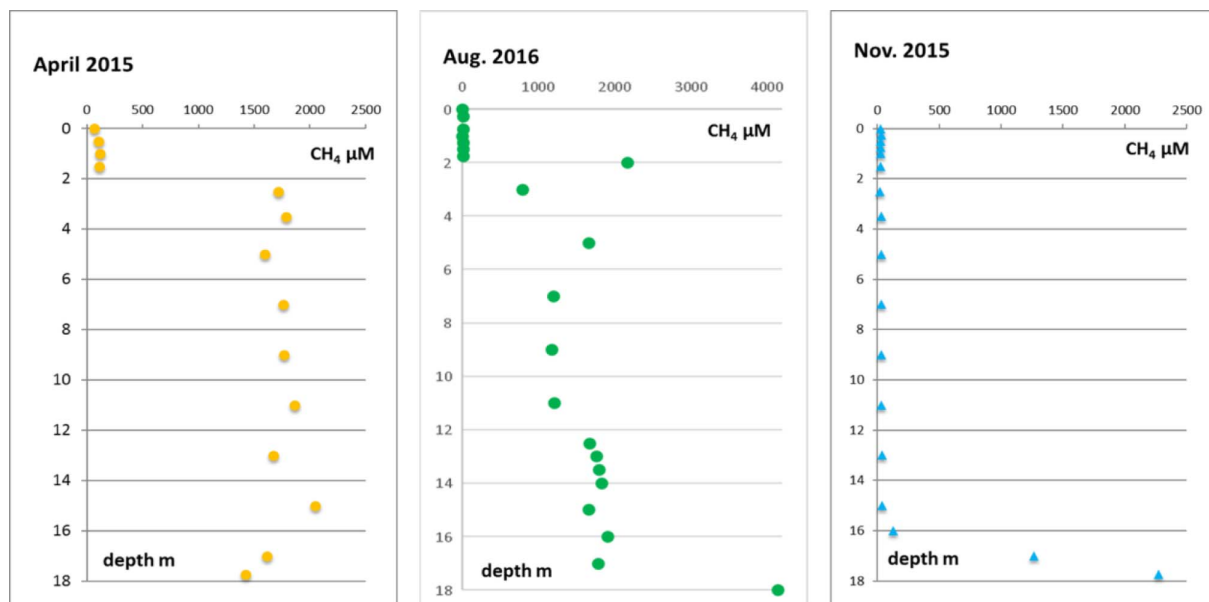


Figure 9. CH₄ profiles obtained at the DS station showing the contrast between (a) stratified (April 2015, August 2016) and (b) non-stratified (November 2015) periods.

Table 4. Averaged Lake/Seawater molar ratios of major dissolved chemical species and alkalinity for the water layer between 2 and 13 m

Na _{lake} /Na _{SW}	K _{lake} /K _{SW}	Si _{lake} /Si _{SW}	Alk _{lake} /Alk _{SW}
2.3 ± 0.2	4.0 ± 0.7	114 ± 7	115 ± 8
Cl _{lake} /Cl _{SW}	Ca _{lake} /Ca _{SW}	Mg _{lake} /Mg _{SW}	SO _{4lake} /SO _{4SW}
1.64 ± 0.05	0.008 ± 0.003	0.08 ± 0.01	0.08 ± 0.02

of rainfall/evaporation/infiltration and from the biological activity that has been at work up to now.

Because evaporation modifies the molar ratio of any dissolved element X_{lake} relative to seawater X_{SW} , the ratios X_{lake}/X_{SW} should reflect concentration/dilution processes as well as geochemical processes that may have changed the lake water composition since its seawater origin. Table 4 displays these ratios for major dissolved species but, in order to apprehend a long-term evolution of the composition of the lake water and eliminate seasonal variations, we consider only the part of the water column located between the halocline and the deep chemocline *i.e.* 2 to 13 m.

These data allow us to classify dissolved chemical elements into four categories according to their ratio X_{lake}/X_{SW} .

- Conservative elements, such as Cl⁻ with a ratio of 1.64 ± 0.5, which is known not to participate in biogeochemical processes. Salinity may also be included in this category, its Lake/SW ratio being of 1.8 ± 0.1, *i.e.*, very close to that of Cl⁻.
- Non-strictly conservative elements: Na⁺, K⁺ with slightly higher Lake/SW ratios than Cl⁻.
- Reactive elements: Ca²⁺, Mg²⁺ and SO₄²⁻ with very low Lake/SW ratios.
- Alkalinity and dissolved silica with very high Lake/SW ratios.

5.4. Strictly conservative elements

The lack of reactivity of Cl⁻ together with the isolation of the ecosystem with respect to the ocean

resulted in the invariability of the initial stock of this element. Salinity was included in the same category since it is a good tracer of physical processes like water mixing, dilution or concentration. In the intermediate part of the water column between the halocline and the deep chemocline, the Cl⁻ concentration and the salinity remain nearly constant whatever the year of sampling (Figures 3 and 6). Therefore, the present Cl_{Lake}/Cl_{SW} = 1.64 ± 0.05 observed today indicates a deficit of meteoric inputs compared to evaporation over the lake history. This deficit is compatible with the present hydrological balance given the uncertainties that affect it. Assuming that both the endorheic character and the present-day climatic conditions can be extrapolated for the whole lake history, we can predict that in the long-term future the lake would eventually dry up, following the concentration processes observed for salt marshes (NaCl saturation) or for Bolivian “salars” sufficiently concentrated to precipitate sylvite and/or natron. To reach this situation the concentration factor of the seawater must approach 90 [Copin-Mont egut, 1996]. The timescale needed to reach such a concentration factor can be calculated assuming isothermal evaporation, which is a diffusion process obeying Fick’s first law. It originates from the difference in chemical potential between the activity of water in the liquid and the gaseous phase (Supplementary 6).

Two “limit models” can therefore be considered:

- an evaporation rate that decreases linearly as a function of time;
- a non-linear evaporation rate.

Using Cl⁻ as the reference species we can write:

$$R(t) = Cl_{lake}/Cl_{SW} \text{ at any time } t, \text{ with } R_0 = 1$$

when the lake formed 4000 years ago.

In the case of a linear model, we can write:

$$R(t) = R_0 + kt, \text{ with } R_0 = 1 \text{ so } R(t) = 1 + kt.$$

With $t = 4000$ years and $R(t) = 1.64 \pm 0.05$, $k = (1.6 \pm 0.1) \times 10^{-4} \text{ yr}^{-1}$.

In the case of a non-linear model, the evolution speed of $R(t)$ decreases as $R(t)$ increases. This is suggested by the ΔG of evaporation process, which increases as evaporation progresses leading to a water which is more and more concentrated. In other words, the evaporation of water requires more and more energy. Since the energy input (irradiance close

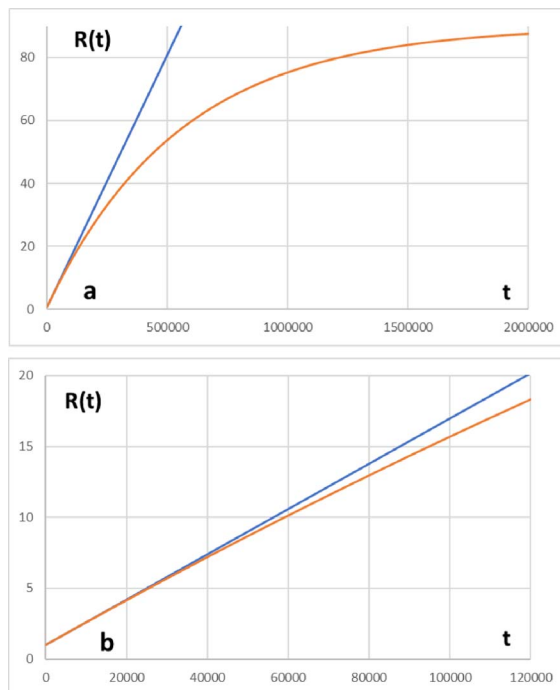


Figure 10. (a) evaporation models. (b) focus showing the divergence between the models after 40 kyr.

to $231 \pm 55 \text{ W}\cdot\text{m}^{-2}$ whatever the season) is not expected to vary much, the rate of evaporation should decrease.

Then we can write:

$$\frac{dR(t)}{dt} = -k \cdot R(t)$$

the integration of which leads to:

$$R(t) = (R_0 - R_\infty) \cdot \exp(-k \cdot t) + R_\infty$$

with limits conditions $R_0 = 1(t = 0)$ and $R_\infty = 90$ ($t \rightarrow \infty$) which corresponds to drying out and natron/sylvite precipitation. The above equation yields $k = (1.8 \pm 0.3) \times 10^{-6} \text{ yr}^{-1}$.

Time evolution of $R(t)$ for both models is shown in Figure 10. Divergence between the two models becomes large when $R(t) > 8$ ($t > 40$ kyr). It is presently impossible due to the lack of additional information, to know which model is the most pertinent. However, the work by Zinke *et al.* [2003] shows that paleogeographic and paleoclimatic conditions have not drastically changed over the last 7000 years period. We can thus assume that these conditions will remain in the future close to the present ones.

5.5. Non-strictly conservative elements: Na and K

The non-strictly conservative behavior of these two elements is evidenced by the $\text{Na}_{\text{Lake}}/\text{Na}_{\text{SW}}$ and $\text{K}_{\text{Lake}}/\text{K}_{\text{SW}}$ ratios significantly higher than those calculated for Cl and salinity. The value of these ratios, respectively of 2.3 ± 0.2 and 4.0 ± 0.7 , show that Na^+ and K^+ are sourced to the lake by weathered minerals from the lake catchment: specifically, clinkstone/phonolitic glasses and pumices, rich in anorthoclase ($\text{Na}_{0.7}\text{K}_{0.3}\text{AlSi}_3\text{O}_8$) [Milesi *et al.*, 2019].

A larger dispersion of the Na and K profiles depending on the sampled year compared to Cl (Figures 5 and 6) for which the lake is considered to be a closed system indicates changes in the inputs of Na and K into the lake, linked to changes of groundwater circulation, which in turn depends on seasonal rainfall. The sink for these two elements is the neoformation of smectites [Milesi *et al.*, 2019] revealed by the XRDP analysis of the first meter of sediment. These are essentially saponites, which can constitute a sink for Na and K, as well as for Mg sourced from the dissolution of the hydromagnesite, abundance of which decreases with depth [Milesi *et al.*, 2019].

5.6. The fate of reactive elements

Elements depleted with respect to seawater: Ca and Mg

It can be reasonably assumed that during initial lake filling calcium and magnesium concentrations were close to those of the current seawater, *i.e.* $10 \text{ mm}\cdot\text{L}^{-1}$ and $53 \text{ mm}\cdot\text{L}^{-1}$ respectively. Since then, these two elements have been continually supplied to the lake by watershed rocks weathering *via* their transfer by phreatic waters. Yet, their actual concentration is very low with respect to seawater (*i.e.* $78 \mu\text{mol}\cdot\text{L}^{-1}$ and $4.4 \text{ mmol}\cdot\text{L}^{-1}$, respectively). The question is what are the geochemical processes that have been at work to ensure that present ratios are so low compared to the initial seawater?

Ca

Given the petrographic environment of the lake catchment, Ca may originate from the dissolution of volcanic glasses rich in plagioclases and other accessory minerals such as amphiboles and pyroxenes. Dissolution of carbonate blocks of coral reef embedded in volcanic ashes is also likely.

Figure 5 shows dissolved calcium profiles obtained for each field survey. Between 3 and 13 m depth, the $\text{Ca}_{\text{Lake}}/\text{Ca}_{\text{SW}}$ ratio is of 8×10^{-3} and the mean concentration of $78 \pm 36 \mu\text{M}$. When the halocline is present, there is a systematic increase and a higher dispersion of the Ca concentration in the vicinity of the surface (0 to 1 m layer), which is not observed for Na, K and Mg. It is likely that this increase is due to the weathering of the microbialites that emerge during the dry season and which are gradually submerged as the water rises during the rainy season. This weathering is enhanced by acid rains, pH of which lies between 4.40 and 5.94. Under these conditions carbonic acid is the main species of DIC and the carbonates of the bio-constructions can dissolve. On the other hand, the water column is supersaturated with respect to aragonite and *a fortiori* to calcite. For example, the saturation coefficient ($\log\Omega$) of calcite and aragonite was respectively 1.2 ± 0.2 and 1.0 ± 0.1 in April 2014, and 1.5 ± 0.1 and 1.3 ± 0.1 in November 2014. The high pH (>9) and the temperature of the water (always close to 30 °C) would have favored the precipitation of these carbonates.

A sampling of the very few centimeters of the sediment done in September 2010 showed that the surface sediment, after combustion of the organic matter, contains 100% of carbonates. XRDP analysis showed that it is only composed of aragonite and hydromagnesite. Ten centimeters below the SWI this proportion falls to $49 \pm 3\%$ owing to the mixing with inherited minerals. Similar paragenesis was observed in all the core samples investigated by Milesi *et al.* [2019].

Mg

Like calcium, magnesium is very depleted with respect to seawater. Within the 3 to 13 m water depth range, the $\text{Mg}_{\text{Lake}}/\text{Mg}_{\text{SW}}$ ratio is 0.08. In addition to aragonite, the other main authigenic carbonate evidenced by XRDP analysis is hydromagnesite $\text{Mg}_5(\text{CO}_3)_4(\text{OH})_2\cdot 4\text{H}_2\text{O}$. It is present at the SWI and it was identified for the first time in March 2009 (Figure 8(b)) in the short sediment core obtained at the CLB station. The Visualminteq software was used to check the saturation coefficient ($\log\Omega$) of this mineral in the water column. The calculated $\log\Omega$ was in the range 1 (August 2016) to 3 (April 2014) in surface water. This does not prove by itself that hydromagnesite precipitates in the water column of lake Dziani

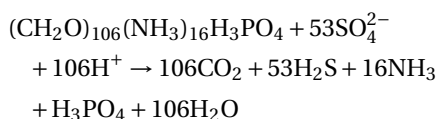
Dzaha because we have no information about the reaction kinetics but it shows that it is thermodynamically possible. However, the occurrence of hydromagnesite in settling particles clearly indicates a neof ormation within the water column. Deeper in the sediment (between 20 and 100 cm depth), a magnesian saponite forms at the expense of hydromagnesite without substantially altering the aragonite sediment content [Milesi *et al.*, 2019].

Thus, carbonate precipitation is the main sink for calcium and a transitional sink for magnesium. This can explain the very low concentrations of both elements compared to the original seawater.

5.7. Depletion of sulfate and sulfur cycle

Sulfate and soluble sulfide ($\Sigma(S-II)$), are the only major sulfur species measured in the water column. With respect to the original seawater, sulfate is presently highly depleted ($SO_4(\text{lake})/SO_4(\text{SW}) = 0.08 \pm 0.02$) while H_2S concentrations are highly variable according to the season. Figure 6 shows that at the end of rainy seasons (April 2012, 2014, 2015) very strong gradients exist at 1.75 m to 2 m depth while when the lake is mixed (November 2014, 2015, 2017) concentrations are very low. On the other hand, the sulfate concentration falls below the detection limit when the H_2S concentration starts to increase (Figure 7). When H_2S exhibits very low concentrations in the top of the water column, the sulfate concentration is always within the range $2400 \pm 450 \mu\text{mol}\cdot\text{L}^{-1}$.

Bacterial sulfate reduction (BSR) can explain the behavior of sulfur species according to the global reaction:



It should also be noted that BSR produces a significant increase in alkalinity and pH since the alkalinity increase is greater than those of DIC ($\Delta\text{Alk}/\Delta\text{DIC} = 1.15$). We show later in the paper that H_2S could also be produced by anaerobic oxidation of methane.

Sulfate in seawater is nearly a conservative element [Copin-Mont gut, 1996]. If this was subject only to precipitation/evaporation cycles, the ratio $SO_{4\text{Lake}}/SO_{4\text{SW}}$ should be close to the one calculated for chloride (1.64 ± 0.05) and the present sulfate concentration would reach about $52 \text{ mmol}\cdot\text{L}^{-1}$

($32 \text{ mmol}\cdot\text{L}^{-1}$ in present-day seawater). The low value of the $SO_{4\text{Lake}}/SO_{4\text{SW}}$ ratio (0.08 ± 0.02) clearly shows that this species is involved in processes that trend to eliminate it from the system.

A question that remains to be solved is why do we observe, whatever the season a nearly constant sulfate concentration of $2400 \pm 450 \mu\text{mol}\cdot\text{L}^{-1}$ in the water column?

If we go back to the original hypothesis which assumes that the lake was originally filled with seawater, there must be a definitive sink for sulfate which has led during 4000–7000 years to its decrease from its initial concentration of $32 \text{ mmol}\cdot\text{L}^{-1}$ in seawater to its current concentration of $2.4 \text{ mmol}\cdot\text{L}^{-1}$.

A simple qualitative experiment done in 2010 on a short sediment core (0 to 10 cm below the SWI) showed that iron could be the definitive sink for sulfate through (i) BSR and (ii) iron sulfide precipitation. This experiment has shown that in contact with air, the sediment gets rusty within a few tens of minutes, attesting to the oxidation of soluble Fe(II) to insoluble Fe(III). On the other hand, drops of concentrated HCl on the sediment led to a strong release of H_2S likely due to iron sulfides dissolution. Then the definitive sink for sulfate can be summarized by an irreversible pathway: $SO_4 \rightarrow \text{BSR}(H_2S) + \text{Fe(II)} \rightarrow \text{FeS}_x$.

Whereas Fe can be permanently supplied through the weathering of the lake catchment, mainly in the form of particulate Fe(III) (oxides and oxyhydroxides are reduced in soluble Fe(II) within the anoxic environment of the lake), it is radically different for sulfate, the stock of which is limited since there are no external sources to the ecosystem.

Then, the current measured concentration ($\sim 2.4 \text{ mmol}\cdot\text{L}^{-1}$ during the homogeneous period or above the halocline when the water column is stratified) represents the remaining fraction of the $32 \text{ mmol}\cdot\text{L}^{-1}$ initially present in the original seawater about 4000–7000 years ago.

At any time t the evolution of the sulfate concentration can be written:

$$\frac{d(\text{SO}_4)}{dt} = \text{regeneration} - \text{consumption}$$

As shown by Berner [1980], a zero-order reaction prevails for BSR (consumption) when the substrate (sulfate) is renewed experimentally. It turns to order 1 when the supply of substrate is limited. Since our ecosystem appears to be closed with respect to sulfate, it is relevant to infer a kinetics order of 1 soon

after the lake has developed a high primary production together with an anoxic zone in the water column.

Several hypotheses can be considered for the writing of the above equation:

1. Order 0 for regeneration: anoxygenic photosynthesis and direct oxidation of HS⁻ by O₂ with a kinetics constant set as k_1 . Evaporation which exists also for sulfate as it does for chloride can be included in the “regeneration” term. Order 1 for consumption with a kinetics constant set as k_2 .
2. Order 1 for regeneration and order 0 for consumption. This hypothesis has no sense because it leads to an increasing SO₄ concentration with time.
3. Order 0 for both regeneration and consumption.
4. Order 1 for both regeneration and consumption.

The hypothesis (1) leads to write:

$$\frac{d(\text{SO}_4)}{dt} = k_1 - k_2(\text{SO}_4)$$

integration of which gives:

$$(\text{SO}_4)_t = (\text{SO}_4)_0 \cdot \exp(-k_2 t) + \frac{k_1}{k_2} \cdot (1 - \exp(-k_2 t)).$$

When $t = 0$, the second term of the right side is 0 and $(\text{SO}_4)_t = (\text{SO}_4)_0$ *i.e.* 32 mmol·L⁻¹.

The second limit condition takes into account the permanent decrease of sulfate concentration due to its initial limited amount and its definitive trapping as FeS in the sediment. Then we can infer that $(\text{SO}_4)_t \rightarrow 0$ as $t \rightarrow \infty$. Reporting this limit condition in the above equation leads to set:

$$(\text{SO}_4)_{t \rightarrow \infty} = \frac{k_1}{k_2}$$

Assuming that BSR is no longer possible when the substrate has reached a concentration as low as 0.01 mmol·L⁻¹ sets the ratio $k_1/k_2 = 0.01$.

Using the above initial conditions and taking into account the present sulfate concentration of 2.4 mmol·L⁻¹ with $t = 4000$ yr we calculate $k_2 = 6.50 \times 10^{-4}$ yr⁻¹ and $k_1 = 6.50 \times 10^{-6}$ yr⁻¹. This returns a half-life for sulfate $t_{1/2} = 1067$ yr. The somewhat arbitrary limit of 10 μmol·L⁻¹ is reached after 20 kyr. The other important uncertainty is that we do not know if the kinetics of the BSR has ever switched from order 0 to order 1 and, if so, when?

The third hypothesis leads to a linear decrease of sulfate: $k_1 - k_2 = -7.4 \times 10^{-3}$ yr⁻¹, with $t_{1/2} = 2160$ yr and the concentration of 10 μmol·L⁻¹ reached after 4300 years *i.e.* within the next 300 years which does not seem very likely.

The last hypothesis (4) returns:

$$(\text{SO}_4)_t = (\text{SO}_4)_0 \cdot \exp(k_1 - k_2) \cdot t$$

With the same initial and present-day conditions, $k_1 - k_2 = -6.47 \times 10^{-4}$ yr⁻¹ which leads to the same results than for the first hypothesis *i.e.* $t_{1/2} = 1067$ yr and a vanishing SO₄²⁻ concentration reached after 20 kyr.

We cannot definitively conclude about the fate of sulfate in the lake. Hypotheses (1), (3) and (4) lead to very different temporal evolutions because we have no data about the kinetics of the regeneration processes. However, it is probably one of these reactional pathways that has led to the present-day concentration. This could result from: (i) a definitive trapping in sulfides, the most likely being iron sulfides, and (ii) an incomplete re-oxidation of sulfide produced by the BSR. An attempt to depict the sulfur cycle and this interactions with carbon and iron is displayed on Figure 11.

6. The carbon cycle

Like in any lacustrine ecosystem, all processes regarding the carbon cycle are driven by exchanges of CO₂ with the atmosphere. The dissolution of this gas generates the DIC and is the primary carbon source which sustains the development of cyanobacteria and part of the microbial population through the photosynthetic bacteria. All the other processes *i.e.* mineralization (oxic and anoxic respiration), organic matter (OM) early diagenesis and authigenic carbonates are directly or indirectly the consequence of the CO₂ dissolution. In addition to atmospheric CO₂ we must add, first, a magmatic contribution, a relic of volcanic activity which is a hallmark of the lake and secondly, the exogenous contribution that results from the mineralization of the plant material transported by the wind. The organic carbon mineralization from phytoplanktonic or exogenous sources causes high concentrations of DOC independent from the season, which reinforces the hypothesis of a permanent input to the ecosystem. If we consider the 3 to 13 m depth range,

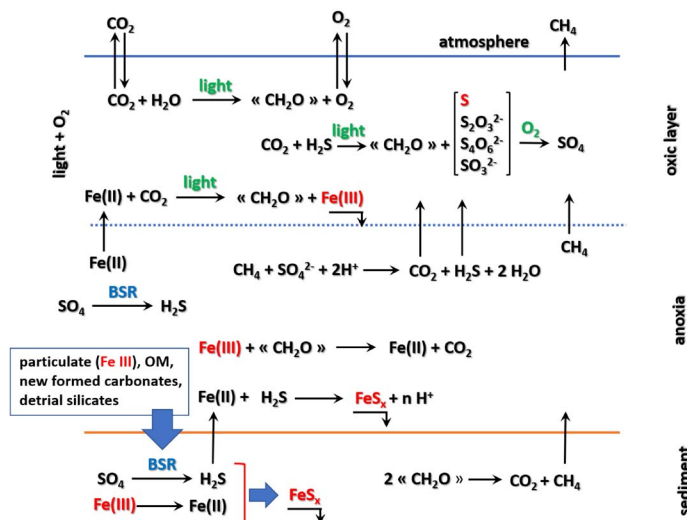


Figure 11. The sulfur cycle and its interactions with these of carbon and iron.

the average DOC concentration calculated for the campaigns 2012 to 2017 is $7328 \pm 815 \mu\text{mol}\cdot\text{L}^{-1}$, a concentration which is about 30 times higher than the local seawater (measured in November 2015).

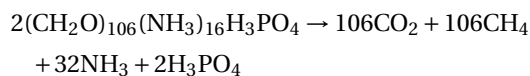
6.1. CO_2 fluxes at the air–water interface

In addition to the measured CO_2 fluxes displayed in Table 1, we have calculated with the software Visualminetq the pCO_2 for the surface water which shows a permanent over saturation with respect to the atmospheric pCO_2 set at $400 \mu\text{atm}$. The saturation coefficient lies between 1.2 to 10. Moreover, direct measurements of CO_2 fluxes show that the degassing of the lake is permanent even during the daytime when photosynthesis is the most active. During the stratified (rainy) periods, the average flux is $80 \pm 35 \text{ mmol}\cdot\text{m}^{-2}\cdot\text{d}^{-1}$ while, during the homogeneous (dry) periods, it is $215 \pm 5 \text{ mmol}\cdot\text{m}^{-2}\cdot\text{d}^{-1}$. This can be explained by differences in diffusion processes: during the stratified period the strong gradient induced by the halocline considerably decreases the dispersion coefficients and opposes the diffusion of CO_2 . Therefore, the water layer above the halocline only contributes to the diffusion of the CO_2 produced by the biomass respiration. Conversely, during a homogeneous period, the CO_2 can diffuse freely towards the atmosphere over the entire height of the water column.

6.2. Origin of CH_4 and fluxes at the air–water interface

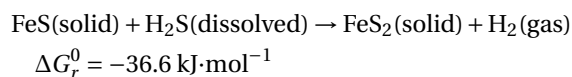
The origin of methane

Methane is a common component of lacustrine ecosystems [Bastviken *et al.*, 2008], being either dissolved or escaping from the water to the atmosphere owing to its very low partial pressure (presently $1.8 \times 10^{-6} \text{ atm}$ and a residence time about 10 years). Methane production in a lake results from the disproportionation of organic matter. Since the main source of organic carbon has a phytoplanktonic origin, we can write the reaction statement as:



However, this statement does not enlighten the main metabolic pathways involved, which are acetogenesis and hydrogenotrophy.

Both processes are microbially mediated by methanogenic Archaeal populations, which are abundant in lake Dziani Dzaha [Hugoni *et al.*, 2018]. For hydrogenotrophy, the hydrogen needed can come from the W achtersh user reaction [Drobner *et al.*, 1990] which operates in a strictly anoxic medium:



H₂S is always present even at weak concentrations, occurrence of FeS have not been proved experimentally but it should be present in the sediment in an amorphous form while pyrite has been evidenced in the sediment and in the stromatolites as framboids.

Measured and calculated methane fluxes

Measured CH₄ fluxes are displayed in Table 1. Fluxes can be calculated with the profiles obtained in April 2015 and August 2016 when the water column was still stratified (Figure 9). Another profile has been obtained in November 2015 when the lake had no halocline: the absence of halocline makes possible the diffusion of oxygen from the surface to the bottom and explain the observed very low concentrations (40 to 120 $\mu\text{mol}\cdot\text{L}^{-1}$). The increasing concentration of CH₄ between 15 m (37 μM) and the lake bottom at DS (2274 μM at 17 m) was due to diffusion from the pore water where CH₄ is continuously produced by organic matter fermentation in sediments. However, CH₄ can also be oxidized at depth through anaerobic reactions which use intermediate sulfur products, as S⁰, if there is no sulfate [Cassarini, 2017, Milucka *et al.*, 2012].

CH₄ profiles observed when the water column was stratified (April 2015 and August 2016) showed very strong gradients located at the halocline. Owing to these very sharp gradients, we can infer that the dispersion coefficient for CH₄ must be close to the molecular diffusion coefficient at 30 $^{\circ}\text{C}$ *i.e.* $2.0 \times 10^{-5} \text{ cm}^2\cdot\text{s}^{-1}$. Then it is possible to calculate the related fluxes with the first Fick's law:

- 1 $\text{mmol}\cdot\text{m}^{-2}\cdot\text{d}^{-1}$ for April 2014
- 1.4 $\text{mmol}\cdot\text{m}^{-2}\cdot\text{d}^{-1}$ for August 2016.

They can be compared with the fluxes measured by the FC method that were 103 $\text{mmol}\cdot\text{m}^{-2}\cdot\text{d}^{-1}$ and 107 $\text{mmol}\cdot\text{m}^{-2}\cdot\text{d}^{-1}$ respectively, which is about 100 times larger than calculated fluxes. Such a discrepancy cannot be attributed to a difference of the dispersion coefficient. Since a concentration peak is observed at the halocline (August 2016), it is likely that methane is produced at this depth by methanogenic Archaea which generate two vertical fluxes downwards and upwards within the water column. For the latter the distance to the surface is too short and the residence time of the methane is too low for it to have time to oxidize or to be consumed by aerobic methanotrophic bacteria, which explains the very high fluxes towards the atmosphere.

These measured fluxes can be compared to what is produced in other lacustrine ecosystems. Walter *et al.* [2006] reported CH₄ fluxes from several lakes in Siberia around 4.4 $\text{mmol}\cdot\text{m}^{-2}\cdot\text{d}^{-1}$ while a study done on 14 lakes by Casper *et al.* [2000] provided values between 1 to 24 $\text{mmol}\cdot\text{m}^{-2}\cdot\text{d}^{-1}$. A more complete bibliographic search never mentions such high values as those measured in Dziani Dzaha which appears as the most methane productive lake ever studied.

Carbon sources and sinks

As a conclusion about the carbon cycle in lake Dziani Dzaha, we can summarize the various sources and sinks for carbon and then try to draw a pattern of its cycle in the ecosystem.

(i) Direct carbon sources

- inorganic: atmospheric and hydrothermal CO₂ inputs
- organic: detrital inputs of terrestrial plants from the watershed (POC and DOC).

(ii) Indirect carbon sources

- aerobic respiration of living organisms and organic matter mineralization (DIC)
- anaerobic respiration of sulfate through BSR (DIC)
- organic matter fermentation (CO₂ + CH₄)
- Mg and Ca carbonates precipitation are sources of CO₂.

Carbon sinks

- oxygenic and anoxygenic photosynthesis
- outgassing of CO₂ and CH₄
- carbonates precipitation because half of the carbon is trapped in the solid for calcite or aragonite and two sevenths for hydromagnesite
- refractory organic matter preserved in the sediment and burial of organic residues.

This inventory does not account for the many interconnections that exist between all biogeochemical processes including interactions with the sulfur cycle through the BSR and the methane oxidation by oxidized sulfur species (S_{ox}).

7. Conclusions

This study of the Lake Dziani Dzaha completes the previous works mainly devoted to the peculiar hydrobiological and biological features of the lake and

help to a better understanding of how this ecosystem works. This lake first appears as a microbial world where highly adapted Archaea, Bacteria and Eukaryota co-exist. Starting from the original seawater, the slow but permanent evaporation has led to a concentrated medium where only specialized microorganisms are able to survive and thrive. In other words, this specific environment leads to sustain a very low biodiversity and has locked any possibility to open any other ecological niche. In some aspects this evolution may remind the primitive ocean at the time of the GOE about 2.4 Gy ago [Canfield *et al.*, 2013].

We showed that the main geochemical processes are oxygenic and anoxygenic photosynthesis, BSR and methanogenesis which, as far as we know, generate the largest methane fluxes ever been recorded in lacustrine aquatic ecosystems.

Future researches will be addressed to improve our knowledge of the biogeochemical functioning of this very peculiar ecosystem; especially, more data concerning microbial processes related to their geochemical and hydrological context are needed.

Then, lake Dziani Dzaha, through its exceptional biogeochemical peculiarities is probably a unique ecosystem if we consider that nothing similar has never been published before 2017.

Consequently, it seems essential that the local institutions responsible for environmental management make the necessary decisions for its protection.

Acknowledgments

Our thanks go to Laure Cordier, Micka l Tharaud and Hassiba Lazar for their essential contribution to the analyzes carried out in the laboratory of the IPGP.

Many thanks also for the two anonymous reviewers who have greatly help to improve the original manuscript.

This work was funded by the Agence Nationale de la Recherche (France) grant no ANR-13-BS06-000, the Universit  Montpellier II (projects METTRO and MYPROBE), and the Total Corporate Foundation (project DZAHA).

Supplementary data

Supporting information for this article is available on the journal's website under <https://doi.org/10.5802/crgeos.43> or from the author.

References

- Aucher, W., Delafont, V., Ponlaitiac, E., Alafaci, A., Agogu , H., Leboulanger, C., Bouvy, M., and H chard, Y. (2020). Morphology and ecology of two new amoebae, isolated from a hypersaline lake, which graze on cyanobacteria. *Protist.* submitted, MS #PROTIS_2020_10.
- Bastviken, D., Cole, J. J., Pace, M. L., and Van de Bogert, M. C. (2008). Fates of methane from different lake habitats: Connecting whole-lake budgets and CH₄ emissions. *J. Geophys. Res.*, 113, article no. G02024.
- Bernard, C. *et al.* (2019). Very low phytoplankton diversity in a tropical saline-alkaline lake, with co-dominance of *Arthrospira fusiformis* (Cyanobacteria) and *Picocystis salinarum* (Chlorophyta). *Microbiol. Ecol.*, 78(3), 603–617.
- Berner, R. A. (1980). *Early Diagenesis. A Theoretical Approach*. Princeton University Press. ISBN 08223-5.
- Canfield, D. E. *et al.* (2013). Oxygen dynamics in the aftermath of the Great Oxidation of Earth's atmosphere. *Proc. Natl Acad. Sci. USA*, 110(42), 16736–16741.
- Casper, P., Maberly, S. C., Hall, G. H., and Finlay, B. J. (2000). Fluxes of CH₄ and CO₂ from a small productive lake to the atmosphere. *Biogeochem.*, 4, 1–19.
- Cassarini, C. (2017). *Anaerobic oxidation of methane coupled to the reduction of different sulphur compounds in bioreactors*. PhD thesis, Univ. Paris Est. NNT: 2017 PESC 1051.
- CEAEQ (2015). Centre d'expertise en analyse environnementale du Qu bec. D termination des sulfures : m thode colorim trique avec le chlorure ferrique et l'oxalate de N,N-dim thyl-p-ph nyl nediamine. MA 300-S12.
- Cellamare, M. *et al.* (2018). Characterization of phototrophic microorganisms and description of new cyanobacteria isolated from the saline-alkaline lake Dziani Dzaha (Mayotte, Indian Ocean). *FEMS Microbiol. Ecol.*, 94(8), article no. fiy108.
- Copin-Mont gut, G. (1996). *Chimie de l'eau de mer*. Institut O canographique. 29 p. ISBN: 2-903581-14-2.
- Drobner, E., Huber, H., W chtersh user, G., Rose, D., and Stett, K. O. (1990). Pyrite formation linked with hydrogen evolution under anaerobic conditions.

- Nature*, 346(6286), 742–744.
- G rard, E. et al. (2018). Key role of alpha proteobacteria and cyanobacteria in the formation of stromatolites of lake Dziani Dzaha (Mayotte, Western Indian Ocean). *Front. Microbiol.*, 9, 796. eCollection 2018.
- Gran, G. (1952). Determination of the equivalent point in potentiometric titrations, part II. *Analyst (London)*, 77, 661–671.
- Hamilton, T. L., Bryant, D. A., and Macalady, J. L. (2016). The role of biology in planetary evolution: cyanobacterial primary production in low oxygen Proterozoic oceans. *Environ. Microbiol.*, 18(2), 325–340.
- Hugoni, M. et al. (2018). Spatiotemporal variations in microbial diversity across the three domains of life in a tropical thalassohaline lake (Dziani Dzaha, Mayotte Island). *Mol. Ecol.*, 27, 4775–4786.
- Julvez, J. (1987). Epid miologie du paludisme et lutte antipaludique   Mayotte (Archipel des Comores, Oc an indien). Evolution de la situation de 1976   1986. Perspectives. *Bull. Soc. Pathol. Exot.*, 80, 505–519.
- Korzun, V. I. (1978). *World Water Balance and Water Resources on the Earth*. Studies and Report in Hydrology. UNESCO, Paris.
- Krienitz, L. and Schagerl, M. (2016). Tiny and tough: microphytes of East African soda lakes. In Schagerl, M., editor, *Soda Lakes of East Africa*. Springer, Cham (Switzerland).
- Lambert, M. and Fr chette, J. L. (2005). Analytical techniques for measuring fluxes of CO₂ and CH₄ from hydroelectric reservoirs and natural water bodies. In Tremblay, A., Varfalvy, L., Roehm, C., and Garneau, M., editors, *Greenhouse Gas Emissions – Fluxes and Processes Environmental Science*. Springer, Berlin, Heidelberg.
- Leboulanger, C. et al. (2017). Microbial diversity and cyanobacterial production in Dziani Dzaha crater lake, a unique tropical thalassohaline environment. *PLoS One*, 12(1), article no. e0168879.
- Milesi, V. P. et al. (2019). Formation of magnesium-smectite during lacustrine carbonates early diagenesis: Study case of the volcanic crater lake Dziani Dzaha (Mayotte – Indian Ocean). *Sedimentology*, 66(3), 983–1001.
- Milucka, J. et al. (2012). Zero valent sulphur is a key intermediate in marine methane oxidation. *Nature*, 491(7425), 541–546.
- Pelleter, A. A., Caro, M., Cordier, C., Bach lery, P., Nehlig, P., et al. (2014). Melilite-bearing lavas in Mayotte (France): An insight into the mantle source below the Comores. *Lithos*, 208–209, 281–297.
- Rishworth, G. M., Perissinotto, R., and Matthew, S. B. (2017). Patterns and drivers of benthic macrofaunal communities dwelling within extant peritidal stromatolites. *Limnol. Oceanogr.*, 62(5), 2227–2242.
- Sanjuan, B. et al. (2008). Estimation du potentiel g othermique de Mayotte : phase 2- tape2. Investigations g ologiques, g ochimiques et g ophysiques compl mentaires, synth se des r sultats. *Rapport BRGM/RP-56802-FR*, 82 p., 18 fig., 3 tbl., 6 ann.
- Smith, D. E., Harrison, S., Firth, C. R., and Jordan, J. T. (2011). The early Holocene sea level rise. *Quaternary Sci. Rev.*, 30, 1846–1860.
- Traineau, H., Sanjuan, B., Brach, M., and Andru, J. C. (2006). Etat des connaissances du potentiel g othermique de Mayotte. *Rapport BRGM/RP-54700-Fr*, 81 p., 31 fig., 2 ann.
- Walter, K. M. et al. (2006). Methane bubbling from Siberian thaw lakes as a positive feedback to climate warming. *Nature*, 443, 71–75.
- Yu, L., Jin, X., and Welle, R. A. (2008). Multidecade Global Flux Datasets from the Objectively Analyzed Air–sea Fluxes (OA Flux) Project: Latent and Sensible Heat Fluxes, Ocean Evaporation, and Related Surface Meteorological Variables. Technical Report OA Flux Projct. *Technical Report (OA2008–01)*, Woods Hole Oceanographic Institution.
- Zinke, J., Reijmer, J. J. G., Thomassin, B. A., Dullo, W. C., Grootes, P., and Erlenkeuser, H. (2003). Postglacial flooding history of Mayotte Lagoon (Comoro Archipelago, southwest Indian Ocean). *Maine. Geol.*, 194, 181–196.